Eur. Phys. J. D **5**, 107–117 (1999)

THE EUROPEAN PHYSICAL JOURNAL D

EDP Sciences

Injection locking properties of a microchip laser

E.G. Lariontsev[1,a], I. Zolotoverkh[1], P. Besnard[2], and G.M. Stéphan[2,b]

[1] Nuclear Physics Institute, Moscow State University, 119899 Moscow, Russia
[2] Laboratoire d'Optronique associé au Centre National de la Recherche Scientifique[c], École Nationale des Sciences Appliquées et de Technologies, 6 rue de Kérampont, 22305 Lannion, France

Received: 1st April 1998 / Accepted: 21 August 1998

Abstract. An injected microchip laser is theoretically studied, with the use of two models: in the first model, which is traditional, the field is represented by a single frequency component in the slowly-varying envelope approximation. In the second model, referred to as the Fabry-Perot model, two field components are considered which are respectively centered around the frequency of an eigenmode of the injected laser and the frequency of the injected field. Computation of locking ranges, bistability do mains are performed and the results compared. They show not only an improved precision of the second model but also a necessity to use it to describe some effects such as the bistable domains in the limits of the locking domains.

PACS. 42.55.Ah General laser theory – 42.55.Rz Doped-insulator lasers and other solid state lasers

1 Introduction

Injection locking of laser oscillations was studied practically since the development of the first lasers. This phenomenon is important in studies of fundamental problems of non-linear dynamics (such as dynamical chaos, synchronization of chaotic oscillations, bifurcations or bistability) and is of interest for controlling and investigating statistical properties of laser radiation (such as intensity and phase noise or squeezing). Injection locking has also a significant applied value for the improvement of characteristics *s* of high-power lasers (in particular, arrays of coupled lasers), for problems of transmission, processing and storage of information. A boom in studies of properties of injected lasers was observed during the last decade and the properties of injected semiconductor lasers were considered in many theoretical and experimental works. A very important parameter of such lasers is the linewidth enhancement factor. This parameter characterizes a phase-amplitude coupling in a laser. In a first publication Lang [1] theoretically studied dynamics of injected semiconductor lasers with account of this factor. Lang showed that it causes two important features of an injected laser when the frequency of the injected light is used as a control parameter: an asymmetric locking range and an instability of injection locking in a considerable part of the locking range [1,2]. First publications on the bistable behavior in injected semiconductor lasers and resonant amplifiers were done by Japanese scientists [3,4]. The bistability was also attributed to the linewidth enhancement factor. The bistability appears due to the non-linear change of the refraction index which is proportional to this parameter. Investigations on properties of injected lasers have demonstrated that there is a considerable difference in bistability and the locking range for two ways of injection: (a) injection on the peak mode [1–5] and (b) injection on side modes [6,7] (the peak mode is the mode of the slave laser with the frequency closest to the maximum of a gain line). In reference [8], polarization bistability induced by optical injection was observed in a vertical-cavity surface-emitting laser. A number of publications concerns the problems of four-wave mixing in injected solid-state lasers [9–12]. This phenomenon is observed outside the locking range. Beating between the injected signal and the intracavity field of the slave laser induces modulation of the population and this modulation leads to the appearance of additional components in the spectrum of laser radiation. The modulation characteristics and the relaxation oscillations in injected semiconductor lasers were studied in references [13–15]. Several publications were devoted to injection locking of semiconductor laser arrays [16–18]. Non-linear dynamics of injected semiconductor lasers is very rich and it is a subject of numerous current studies (see, for example, Refs. [15,20–28]). Bifurcations, different routes to chaos, formation and properties of strange chaotic attractors were studied in these references. Formation of spatial patterns in lasers subject to optical injection was studied theoretically in references [29,30]. The quantum theory of the intensity- and phase noises and the formation

[a] e-mail: `lar@lfsl2.npi.msu.su`
[b] e-mail: `stephan@enssat.fr`
[c] URA 6082

of non-classical states (in particular, squeezing) in injected solid-state lasers were considered in references [31–33]. The intensity noise near the quantum noise limit was experimentally studied in an injection-locked cw Nd:YAG non-planar ring laser [34]. All the theoretical studies were essentially done on Class-B lasers in the context of the Slowly-Varying Envelope Approximation (SVEA). The field and the population difference obey two coupled nonlinear equations. Another idea has recently been developed in which the field in the injected laser was split into two components playing each the role of a competing dynamic variable [35,36]. We will refer to this model as the Fabry-Perot (F-P) amplifier model. This point of view led to the interpretation of frequency locking as a consequence of a quenching of the gain of the laser mode by the injected field. It allowed also to compute the bistable domains which limit the locking range. These results were experimentally verified using a Class-A laser (a He–Ne laser working at 3.39 μm). One aim of this paper is to apply this idea to Class-B lasers. Recent progress in the development of monolithic ring solid-state and microchip lasers is drawing attention to investigate injection locking for such lasers. The goal of our investigations is a theoretical study of injection locking dynamics of solid-state lasers, in particular microchip lasers. For this purpose, we will develop our model for the injected laser and compare it to the traditional rate-equation model. Injection locking range and periodic beat regime together with their stability will be studied in the rate-equation model. Then the Fabry-Perot amplifier model will be used: comparison of these results with the former case show either an improvement of the former theoretical predictions for some values of the control parameters domains or even an inadequacy of the rate equation model for other values.

2 Two models for injected solid-state laser

In most cases, dynamics of an injected laser was considered within the framework of semi-classical laser theory. Two models for an injected laser were used: the common rate-equation model [1–11,13–28] and the Fabry-Perot amplifier model [35–38]. For a class-B laser system, the polarization of the gain medium is adiabatically eliminated and one deals with two rate equations (for the complex oscillating field within the laser cavity and for the population inversion density). In the case of a single-mode solid-state laser with an external optical signal injected into the resonator, one can write the rate equations in the following form:

$$\frac{d\mathcal{E}}{dt} = \Big[\Gamma\Big(N\frac{1-i\delta}{1+\delta^2}-1\Big) - i(\omega_{in}-\omega_n)\Big]\mathcal{E} + \kappa\frac{\mathcal{E}_{in}}{T_c}, \tag{2.1}$$

$$\frac{dN}{dt} = \frac{1}{T_1}\Big[N_0 - N\Big(1+\frac{Y}{1+\delta^2}\Big)\Big]. \tag{2.2}$$

In the above equations a complex electric field E is represented in the SVEA as: $E = \mathcal{E}\exp(i\omega_{in}t)$. $\mathcal{E}$ and $\mathcal{E}_{in}$ are the complex amplitudes of the electric field, respectively, of the cavity longitudinal mode and of the injected light (κ is the proportion of internal injected field with respect to the external incident field); $Y = |\mathcal{E}|^2$ is the normalized intensity; Γ is the loss rate, T_c is the round-trip time of the cavity. N is the normalized population inversion density, which relaxes with a characteristic time T_1. We assume that the gain line is homogeneously broadened with a central frequency ω_0 and a linewidth $2\gamma_{ud}$; $\delta = (\omega_n - \omega_0)/\gamma_{ud}$ is the relative detuning of the resonant frequency ω_n of the cavity longitudinal mode with respect to the line center. Only one longitudinal mode with the frequency ω_n the closest to the frequency ω_{in} of the injected light is considered. The population inversion density is normalized to its threshold value for lasing at line center. The pump rate is also normalized to its threshold value at $\delta = 0$ and written in the form $N_0/T_1 = (1+\eta_0)/T_1$, where η_0 is a pump excess above threshold at line center.

In references [35–37], the Fabry-Perot amplifier model in which the laser is interpreted as a non-linear amplifier and filter was used for the description of an injected laser. The basic equations of an injected solid-state laser in this model are the following:

$$\frac{d\mathcal{E}_1}{dt} = \Gamma\Big[N\frac{1-i\delta}{1+\delta^2}-1\Big]\mathcal{E}_1, \tag{2.3}$$

$$\frac{d\mathcal{E}_2}{dt} = \frac{1}{T_c}\Big[K\exp(-iF)-1\Big]\mathcal{E}_2 + \frac{\kappa}{T_c}\mathcal{E}_{in}, \tag{2.4}$$

$$\frac{dN}{dt} = \frac{1}{T_1}\Big[N_0 - N\Big(1+\frac{Y_1}{1+\delta^2}+\frac{Y_2}{1+\delta_{in}^2}\Big)\Big] \tag{2.5}$$

where:

$$K = \exp\Big[\Gamma T_c\Big(\frac{N}{1+\delta_{in}^2}-1\Big)\Big] \tag{2.6}$$

$$F = \Big[\omega_{in} - \omega_n + \Gamma N\frac{\delta_{in}}{1+\delta_{in}^2}\Big]T_c. \tag{2.7}$$

$\delta_{in} = (\omega_{in}-\omega_0)/\gamma_{ud}$ is the relative detuning between the injected frequency ω_{in} and the frequency of gain-line center ω_0. $Y_1 = |\mathcal{E}_1|^2, Y_2 = |\mathcal{E}_2|^2$ are the normalized intensities. In this model, the time evolution of a complex electric field E is represented by a sum of two components having carrier frequencies ω_n and ω_{in}:

$$E = \mathcal{E}_1\exp(i\omega_n t) + \mathcal{E}_2\exp(i\omega_{in}t). \tag{2.8}$$

Here ω_n is the frequency of the cavity longitudinal mode closest to the line center (the peak mode). The frequency of injected light is arbitrary. In particular, it can be close to the cavity longitudinal mode which is different from the peak mode. The derivation of these basic equations for both models is given in Appendices A and B.

One of the aims of the present paper is to compare the results obtained by using both models and to investigate their conditions of validity.

3 Rate-equation model

3.1 Injection locking range and stability of stationary locking

In this section, injection locking for the case of the peak-mode injection is considered on the basis of the rate-equation model. Stationary injection locking is described by the stationary solutions of equations (2.1, 2.2). In this case the laser operates at the frequency of the injected signal. The normalized locked field intensity Y and the stationary value of N are expressed as:

$$S^2 = Y\Big[\Big(\frac{N}{1+\delta^2}-1\Big)^2 + \Big(\Omega+\delta\Big(\frac{N}{1+\delta^2}-1\Big)\Big)^2\Big], \tag{3.1}$$

$$N = \frac{1+\eta_0}{1+Y/(1+\delta^2)}, \tag{3.2}$$

where $S = \kappa\mathcal{E}_{in}/(\Gamma T_c\sqrt{I_s})$ is the normalized amplitude of the injected light (κ is the injection coefficient (see Appendix A) and I_s is the saturation parameter (see Appendix B)), $\Omega = (\omega_{in}-\omega_L)/\Gamma$ is the detuning, normalized to the cavity losses Γ, of the injected light frequency from the free-lasing frequency ω_L of the slave laser. Equations (3.1, 3.2) lead to a single cubic equation for Y (or for N).

In the absence of the external light injection, the population inversion density is equal to its threshold value $N_{th} = 1+\delta^2$ (this is obtained from Eq. (2.1) in stationary regime), the normalized intensity Y is $Y_L = \eta_0 - \delta^2$.

The injection locking range is usually defined as the range of detunings Ω where the inequality $Y > Y_L$ holds. Using this definition, the following expressions for the locking range can be derived as it was done in references [1,2].

If $\delta < 0$:

$$-\frac{S\sqrt{1+\delta^2}}{\sqrt{\eta_0-\delta^2}} \le \Omega \le \frac{S}{\sqrt{\eta_0-\delta^2}}\,. \tag{3.3}$$

As it was shown in [1,2] for semiconductor lasers, stable locking can be achieved only in a part of the locking range. The stability of stationary locking was studied by linearization of equations (2.1, 2.2) with respect to small deviations from stationary state. For solutions of the linearized equations proportional to $\exp(\lambda t\Gamma)$, one can derive the following characteristic equation:

$$\lambda^3 + a_2\lambda^2 + a_1\lambda + a_0 = 0, \tag{3.4}$$

where:

$$a_2 = b - 2N_1, \tag{3.5}$$

$$a_1 = N_1^2 - 2bN_1 + N_2^2 + N_3, \tag{3.6}$$

$$a_0 = b(N_1^2+N_2^2) - N_3(N_1+\delta N_2). \tag{3.7}$$

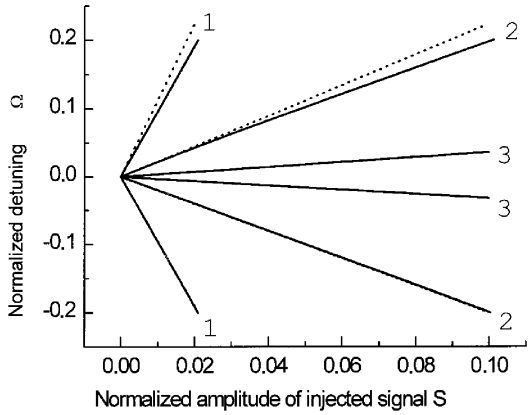

Fig. 1. Locking range boundaries *versus* the normalized amplitude S of the injected field for a YAG:Nd microchip laser for three different values of the pump excess η_0: $\eta_0-\delta^2 = 0.01$ (label 1); $\eta_0-\delta^2 = 0.25$ (label 2); $\eta_0-\delta^2 = 9.84$ (label 3). Dotted curves show the boundaries of the locking range calculated with formula (3.3). Solid lines show boundaries for stability of stationary locking calculated using inequalities (3.12).

where:

$$b = \frac{1}{\Gamma T_1}\Big(1+\frac{Y}{1+\delta^2}\Big), \tag{3.8}$$

$$N_1 = \frac{N}{1+\delta^2} - 1, \tag{3.9}$$

$$N_2 = \delta N_1 + \Omega, \tag{3.10}$$

$$N_3 = \frac{1}{\Gamma T_1}\frac{2NY}{(1+\delta^2)^2}\,. \tag{3.11}$$

In (3.5–3.11) N and Y are the solutions of equations (3.1, 3.2). In accordance with Hurwitz's theorem, the stationary locking is stable if:

$$a_0 > 0, \quad a_1 > 0, \quad a_1a_2 - a_0 > 0. \tag{3.12}$$

Figure 1 shows the locking range boundaries *versus* the normalized amplitude S of the injected field. S is used here as the control parameter. These results were calculated for a YAG:Nd microchip laser having a cavity length of 1 mm, with $\delta = 0.4$, a resonator loss of 2%, and three different values of the pump excess η_0: $\eta_0-\delta^2 = 0.01$ (1); $\eta_0-\delta^2 = 0.25$ (2); $\eta_0-\delta^2 = 9.84$ (3). The dotted curves show the boundaries of the locking range calculated with formula (3.3). The solid lines show boundaries for stability of stationary locking which were calculated using inequalities (3.12). For $\eta_0-\delta^2 = 9.84$ (curves 3), dotted and solid lines coincide. One can see from Figure 1 that stationary locking is stable practically in the whole locking range.

3.2 Bistability within the locking range

In some region of laser parameters there are three stationary solutions of equations (3.1, 3.2). Two of them may be stable simultaneously. In this case bistable injected laser

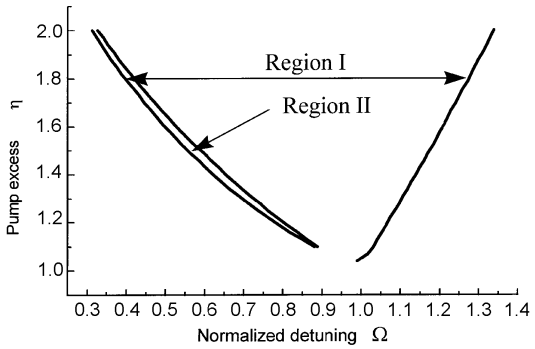

Fig. 2. In region (I) coexist three stationary solutions of equations (3.1, 3.2). Included inside region (I) is the bistability region (II). This diagram is constructed in the plane of parameters (η_0, Ω), for the value $\delta = -1$. These results were computed for a YAG:Nd microchip laser with a cavity length $L = 0.4$ mm and a resonator loss of 2%.

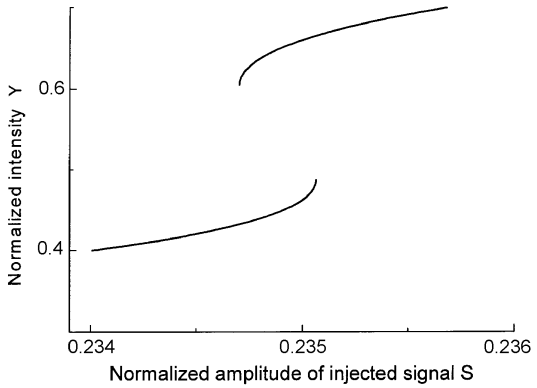

Fig. 3. Bistable intensity within the locking range for a YAG:Nd microchip laser with a cavity length $L = 0.4$ mm, a resonator loss of 2%, $\delta = -1$, $\eta_0 - \delta^2 = 0.4$ and normalized detuning $\Omega = 0.63$.

output can be observed. As it was shown for semiconductor lasers, optical bistability is based on a saturation-induced refractive index change due to light injection. In a solid-state laser, the refractive index change is proportional to δ. At small values of δ ($\delta < 0.5$) this change is thus small and bistability does not clearly appear. We have found regions of laser parameters where three stationary solutions of equations (3.1, 3.2) exist simultaneously and, using the conditions (3.12) for the stability of stationary locking, found the regions in which bistability arises. The results show that at $|\delta| < 1$ bistability arises in very narrow regions of the frequency detunings Ω. Figure 2 illustrates these results, in the plane of parameters (η_0, Ω), for the value $\delta = -1$. Three stationary solutions of equations (3.1, 3.2) exist simultaneously in region (I). In a small part (II) of this region, two of these coexisting solutions are stable and bistability appears. One can reach the value $|\delta| = 1$ for the mode closest to the line center in the case of a YAG:Nd microchip laser with a cavity length $L = 0.4$ mm. In this case $1/T_c = c/(2Ln) = 200$ GHz, $\gamma_{ud} = 90$ GHz and $\delta_{max} = 1/2\gamma_{ud}T_c = 1.1$.

This bistability within the locking range is illustrated in Figure 3 where the laser intensity is displayed as a function of the injected intensity used as a control parameter. The usual S-shaped bistable characteristic curve appears with the lower and upper stable branches.

3.3 Periodic beat regime and its stability

Outside the locked region, the injected field and the laser field are simultaneously present and oscillate at different frequencies. In this region, frequency generation arises through the process of non-linear interaction [9–12]. Injecting a field induces two symmetric frequencies around the laser mode, the first is regeneratively amplified sideband at the injection frequency and the second is a four-wave mixing (FWM) sideband equally and oppositely shifted with respect to the laser frequency.

Analytic solutions describing characteristic s of the injected laser with account of FWM can be found in references [9–12]. These results are valid in the case of weak injected signals. The injected signal S is considered to be weak if the locking bandwidth is less than the relaxation oscillation frequency $\omega_r = [(2\Gamma/T_1)(\eta_0 - \delta^2)]^{1/2}$. In this case the following inequality holds:

$$S < S_0 = \frac{\eta_0 - \delta^2}{[2\Gamma T_1]^{1/2}} \cdot \tag{3.13}$$

For example, if $\eta_0 = 0.5, \delta = 0.5, L = 1$ mm and cavity losses of 2%, one finds $S_0 = 0.002$.

The efficiency in the FWM process resonantly increases when the detuning Ω approaches the relaxation oscillation frequency ω_r. For detuning values larger than ω_r, the FWM efficiency rapidly decreases. We shall thus consider sufficiently strong injected signals $S > S_0$ when the detuning values exceed the relaxation oscillation frequency. In this case the FWM sidebands are negligible as compared to spectral components of injected and laser fields. Neglecting the FWM sidebands, one can write the complex electric field E in the following form:

$$E = \mathcal{E}_1 e^{i\omega_L t} + \mathcal{E}_2 e^{i\omega_{in} t}, \tag{3.14}$$

where $\mathcal{E}_1$ and $\mathcal{E}_2$ are slowly varying amplitudes, and $\omega_L = \omega_n - \delta\Gamma$. The following equations can be derived from (2.1) for the amplitudes $\mathcal{E}_1$ and $\mathcal{E}_2$:

$$\frac{d\mathcal{E}_1}{dt} = (1 - i\delta)\Gamma n\mathcal{E}_1, \tag{3.15}$$

$$\frac{d\mathcal{E}_2}{dt} = (1 - i\delta)\Gamma n\mathcal{E}_2 - i(\omega_{in} - \omega_L)\mathcal{E}_2 + \frac{\kappa E_{in}}{T_c} \cdot \tag{3.16}$$

Neglecting the modulation of N at the difference frequency $\omega_{in} - \omega_L$, equation (2.2) gives:

$$\frac{dn}{dt} = \frac{1}{T_1}\Big[\frac{1 + \eta_0}{1 + \delta^2} - (1 + n)\frac{1 + Y_1 + Y_2}{1 + \delta^2}\Big], \tag{3.17}$$

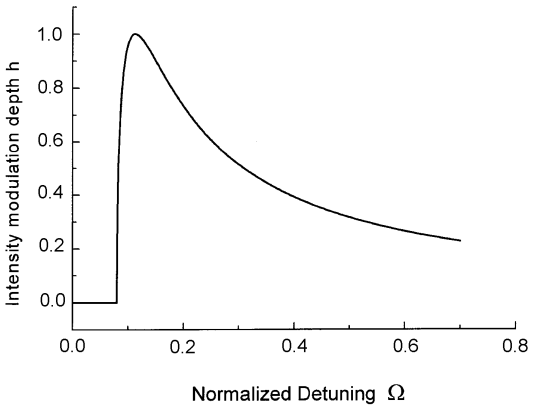

Fig. 4. Intensity modulation depth h *versus* Ω in the periodic beat regime. The results were computed for a YAG:Nd microchip laser with a cavity length $L = 1$ mm, a resonator loss of 2%, $\delta = 0.4$, $\eta_0 - \delta^2 = 0.25$, and a normalized amplitude of the injected field S =0.04.

where $n = N/(1 + \delta^2) - 1$. The stationary solution of equations (3.15–3.17) is:

$$n = 0, \tag{3.18}$$

$$Y_1 = \eta_0 - \delta^2 - Y_2, \tag{3.19}$$

$$Y_2 = S^2/\Omega^2. \tag{3.20}$$

This solution gives the periodic solution of equations (2.1, 2.2), which can be written as:

$$Y_2 = Y[1 + h\cos((\omega_{in} - \omega_L)t + \phi)], \tag{3.21}$$

where:

$$Y = \eta_0 - \delta^2, \tag{3.22}$$

$$h = \frac{2S}{(\eta_0 - \delta^2)\Omega}[\eta_0 - \delta^2 - S^2/\Omega^2]^{1/2}. \tag{3.23}$$

One can see from equations (3.21, 3.22) that the injection induced modulation is characterized by a beat frequency equal to the detuning $\omega_{in} - \omega_L$ and by a mean value of laser intensity similar to that (Y_L) of the free-running laser. The intensity modulation depth h is plotted in Figure 4 as a function of Ω. The periodic solution (3.21–3.23) exists in the range of detunings Ω where inequality $Y_1 > 0$ holds:

$$\frac{S}{[\eta_0 - \delta^2]^{1/2}} < \Omega < -\frac{S}{[\eta_0 - \delta^2]^{1/2}}\,. \tag{3.24}$$

One of these boundaries coincides with the boundary of the stationary locking range (see Eq. (3.3)). In the range of laser parameters where the inequality $|\omega_{in} - \omega_L| \gg \omega_r$ holds, one can find an approximate solution of equations (3.15–3.17) for the nonstationary beat regime. Neglecting the derivative $d\mathcal{E}_2/dt$, one has from (3.16):

$$Y_2 = \frac{S^2}{\Omega^2}\Big[1 - 2\frac{\delta n}{\Omega}\Big]. \tag{3.25}$$

Substituting (3.25) in equations (3.15, 3.17), one can write the following equations:

$$\frac{dY_1}{dt} = 2\Gamma n Y_1, \tag{3.26}$$

$$T_1\frac{dn}{dt} = \frac{1+\eta_0}{1+\delta^2} - (1+n)\Big[1 + \frac{Y_1 + (S^2/\Omega^2)(1 - 2\delta n/\Omega)}{1+\delta^2}\Big]. \tag{3.27}$$

The stability of the beat regime can be studied by linearization of equations (3.26, 3.27) with respect to small deviations from stationary state. The roots of the characteristic equation (Lyapunov exponents) are written as:

$$\lambda_{1,2} = \gamma \pm i\omega_r, \tag{3.28}$$

where the decrement (increment) γ is:

$$\gamma = -\frac{1}{T_1}\Big[\frac{1+\eta_0}{1+\delta^2} - \frac{2\delta S^2}{\Omega^3(1+\delta^2)}\Big], \tag{3.29}$$

and the relaxation oscillation frequency ω_r is:

$$\omega_r = \Big[\frac{2\Gamma}{T_1}\frac{\eta_0 - \delta^2 - S^2\Omega^2}{1+\delta^2}\Big]^{1/2}. \tag{3.30}$$

It should be noted that ω_r in the beat regime is dependent on the beat frequency Ω and decreases to zero at the boundary of the stationary locking range ($\Omega = S/(\eta_0 - \delta^2)^{1/2}$). The periodic intensity beat is stable if:

$$1 + \eta_0 > 2\delta\frac{S^2}{\Omega^3}\,. \tag{3.31}$$

In accordance with (3.31), there is an asymmetry in the stability domain of the periodic intensity beat. When $\delta > 0$, this regime is stable for negative values of detuning Ω. At positive values of Ω, the periodic beat regime is unstable when Ω is such that:

$$\frac{S}{(\eta_0 - \delta^2)^{1/2}} < \Omega < \Big[\frac{2\delta S^2}{1+\eta_0}\Big]^{1/3}. \tag{3.32}$$

The regions of stability for various lasing regimes are shown in Figure 5 in the plane (S, Ω). Numerical solutions of equations (2.1, 2.2) show periodic spiking and the onset of dynamic chaos in the region of instability of periodical beat regime. In numerical simulations, the following values of laser parameters were used: $\eta_0 = 0.5, \delta = 0.5, S = 0.04$, and $\Gamma T_1 = 500$. In accordance with results obtained above, the periodic beat regime is unstable at the values of detuning $\Omega < \Omega_B = \Big[\frac{2\delta S^2}{1+\eta_0}\Big]^{1/3}$. For these values of laser parameters, one has $\Omega_B = 0.102$. For the chaotic regime, the typical time domain behavior of the normalized intensity Y is shown in Figure 6a at the value of detuning $\Omega = 0.1$. Figure 6b shows the time domain behavior for periodic spiking at $\Omega = 0.085$. For detunings Ω outside the locking range, one can observe bistable characteristic s in the microchip laser at values of $|\delta| < 0.5$. The bistability

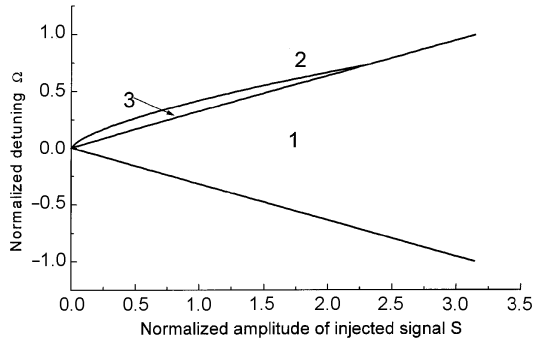

Fig. 5. Regions of stability for various lasing regimes in the plane (S, Ω). The results were computed for a YAG:Nd microchip laser with a cavity length $L = 1$ mm, a resonator loss of 2%, $\delta = 0.4$, $\eta_0 - \delta^2 = 9.84$. Regions 1, 2, and 3 represent, respectively, the stable locking range, the periodic intensity beat, and the chaotic or periodic spiking regime.

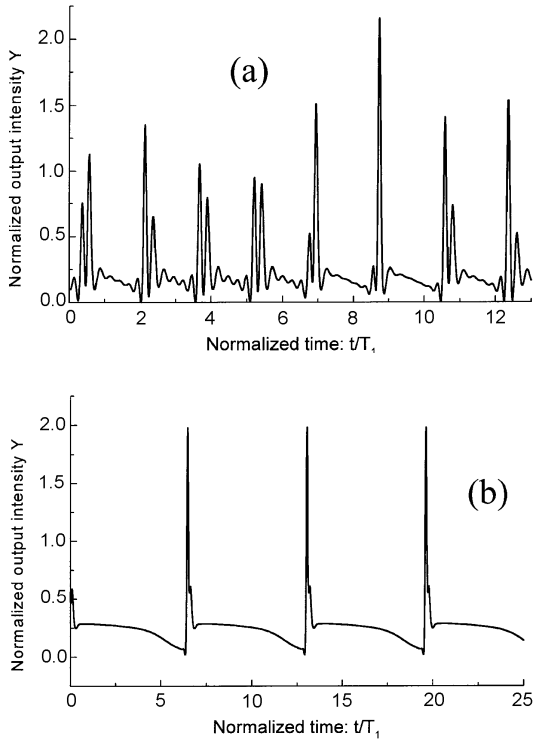

Fig. 6. Time domain behavior of the normalized intensity Y: (a) dynamic chaotic regime for a detuning $\Omega = 0.1$ and (b) periodic spiking at $\Omega = 0.085$.

occurs inside the region of the stable periodic beat regime (region 2 in Fig. 5). The bistable region joins the region of instability of the beat regime (region 3 in Fig. 5). One of these regimes is the periodic intensity beat. Decreasing Ω one can observe the instability of this regime and the transition to chaos at $\Omega < \Omega_B$. Then, the chaotic regime remains for values of detuning $\Omega > \Omega_B$. Near the boundary of stability of the periodic beat regime at $\Omega > \Omega_B$, two regimes (periodic beat and dynamic chaos) can coexist.

4 Fabry-Perot amplifier model

4.1 Injection locking range and stability of stationary locking

In this section, injection locking is considered on the basis of the Fabry-Perot (F-P) amplifier model and the comparison is done with the results obtained with the rate equation model. Stationary injection locking is described by the stationary solutions of equations (2.3–2.5). In this case the laser oscillation is quenched by the injected signal and thus $Y_1 = 0$. Separating the real and imaginary parts of equation (2.4) and summing their quadrates, one obtains the injected stationary intensity inside the laser:

$$Y_2 \frac{1 + K^2 - 2K\cos F}{(\Gamma T_c)^2} = S^2, \tag{4.1}$$

where:

$$K = \exp[\Gamma T_c(N/(1 + \delta_{in}^2) - 1)], \tag{4.2}$$

$$F = [\omega_{in} - \omega_n + \Gamma\delta_{in}N/(1 + \delta_{in})^2)]T_c. \tag{4.3}$$

The stationary value of N is expressed from equation (2.5) as

$$N = \frac{1 + \eta_0}{1 + Y_2/(1 + \delta_{in}^2)} \cdot \tag{4.4}$$

Equations (4.1, 4.4) are analogous to equations (3.1, 3.2) which were derived in Section 3. The phase shift $F_1 = \omega_{in}T_c$ is close to $2p\pi$ (p is an integer) in the case of small detunings $|\omega_{in} - \omega_n| \ll 2\pi/T_c$. In this case equations (3.1, 3.2) coincide with equations (4.1, 4.4). In accordance with equation (2.3), stationary injection locking is unstable if the inequality $N > 1 + \delta^2$ holds. Here $\delta = (\omega_n - \omega_0)/\gamma_{ud}$ is the relative detuning of the peak-mode frequency ω_n from line center. Boundaries for stability of stationary locking can be found from equations (4.1–4.4) in the following way. For $N = 1 + \delta^2$, one has:

$$Y_2 = Y_{20} = (\eta_0 - \delta^2)\frac{1 + \delta_{in}^2}{1 + \delta^2}, \tag{4.5}$$

$$K = K_0 = \exp[\Gamma T_c((1 + \delta^2)/(1 + \delta_{in}^2) - 1)], \tag{4.6}$$

$$F = F_0 = [\Omega - \delta + \delta_{in}(1 + \delta^2)/(1 + \delta_{in}^2)]\Gamma T_c. \tag{4.7}$$

One can write δ_{in} as:

$$\delta_{in} = \delta + \Gamma\frac{\Omega - \delta}{\gamma_{ud}} \cdot \tag{4.8}$$

Substituting (4.5–4.7) into (4.1), one finds:

$$S^2 = F(\Omega) = Y_{20}\frac{1 + K_0^2 - 2K_0\cos F_0}{(\Gamma T_c)^2} \cdot \tag{4.9}$$

One can directly calculate the locking range boundaries Ω *versus* the normalized amplitude S of the injected field by using formula (4.9). Let us first consider the case of injection on the peak-mode (the injected frequency ω_{in} is

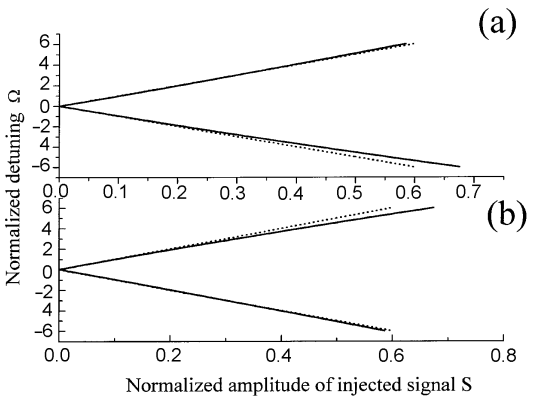

Fig. 7. Locking range boundaries *versus* normalized amplitude S of the injected field for the case of injection close to the peak-mode. Dotted curves show the boundaries of the locking range in the rate equation model. Solid curves show corresponding results of the F-P amplifier model. These results were calculated for the YAG:Nd microchip laser with a cavity length of 1 mm, $\delta = -0.4$ (a) and $\delta = 0.4$ (b), a cavity loss of 10%, and a pump excess $\eta_0 - \delta^2 = 0.01$.

close to the frequency ω_n of the peak mode). The numerical results for the locking range boundaries are plotted in Figure 7. Here the boundaries of locking range calculated with the rate equations model are also shown by dotted curves. Solid curves show corresponding results computed with the F-P amplifier model. These results were calculated for the microchip laser on YAG:Nd with a cavity length of 1 mm, $\delta = -0.4$ (Fig. 7a) and $\delta = 0.4$ (Fig. 7b), a cavity loss of 10%, and a pump excess $\eta_0 - \delta^2 = 0.01$. A loss of 10% was taken to illustrate the appearance of different results given by the rate-equation and F-P amplifier models. For cavity losses less than 10%, boundaries of the injection locking range, computed with the rate-equation and F-P amplifier models, coincide in the considered region of normalized amplitudes S and detunings $\omega_{in} - \omega_n$ such that: $|\omega_{in} - \omega_n| \ll 2\pi/T_c$. Results are plotted in Figure 8 for broader detunings ($|\omega_{in} - \omega_n| \sim 2\pi/T_c$). These results were calculated for $\delta = 0.4$ (Fig. 8a), a cavity loss of 2% and otherwise for the same parameters as before; in Figure 8b, the cavity length is $L = 10$ mm, $\delta = 0$ and other parameters are the same. The dotted curves in Figure 8a show the boundaries of the locking range calculated in the rate-equation model for the case of the peak-mode injection. One can see from Figure 8 that the F-P amplifier model describes not only injection locking on the peak mode but also side-mode injection locking. Boundaries of all ranges of side-mode injection locking are described by formula (4.9). In the rate-equation model, side-mode injection needs a special consideration [6,7]. In the case of small detunings between the injected frequency (ω_{in}) and the cavity-mode frequency (ω_n) ($|\omega_{in} - \omega_n| \ll 2\pi/T_c$) both models give the same results. For larger detunings ($|\omega_{in} - \omega_n| \sim 2\pi/T_c$), the rate-equation model (based on Eqs. (2.1, 2.2)) is not valid and one should use equations (2.3–2.5). The consideration of bistability within the locking range shows that the bistability region in the F-P amplifier model is broader than in the

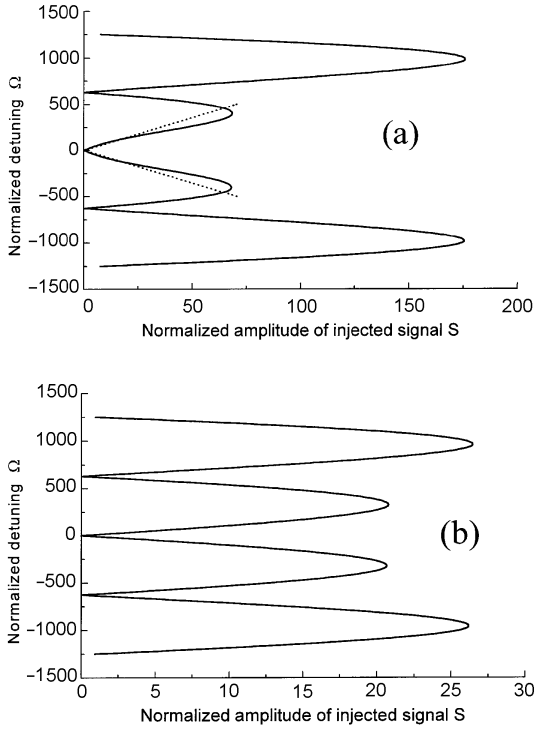

Fig. 8. Locking range boundaries *versus* the normalized amplitude S of the injected field in a broad region of detunings Ω, which includes side-mode injection. The dotted curves show the boundaries of the locking range calculated in the rate-equation model for the case of the peak-mode injection. Solid curves show the results computed by using formula (4.9) of the F-P amplifier model. These results were calculated for a microchip laser with a cavity length of 1 mm, $\delta = 0.4$ (a) and with a cavity length of 10 mm, $\delta = 0$ (b), a cavity loss of 2%, and a pump excess $\eta_0 - \delta^2 = 0.01$.

rate-equation model. The comparison of results obtained in both models is given in Figure 9 in the plane (η_0, Ω). These results were calculated for the YAG:Nd microchip laser with a cavity length of 0.4 mm, $\delta = -1$ and a cavity loss of 2%. There are regions where three stationary solutions for injection locking exist simultaneously. These regions are marked by RE-I and F-P I, correspondingly, for the rate-equation and the F-P amplifier model. Figure 9 shows that the positions of regions RE-I and FP-I are completely different: they are shifted from each other by an amount of detuning (Ω) which exceeds the width of these regions. Within regions RE-I and FP-I, regions of bistability RE-II and FP-II are shown where two coexisting solutions are stable. The bistability region in the F-P amplifier model is much broader. In these calculations, the inequality $N > 1 + \delta^2$ was used as the condition for stability of stationary injection locking.

4.2 Periodic beat regime

In this section, the periodic beat regime is considered on the basis of the Fabry-Perot amplifier model and the results are compared with those obtained with the rate-equation model. The stationary beat regime is described

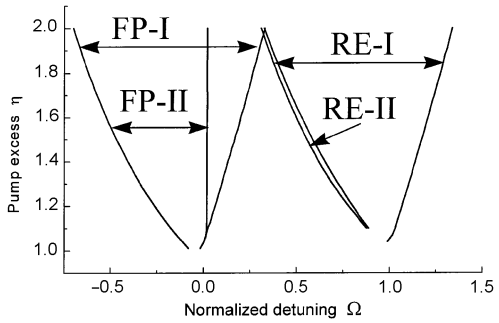

Fig. 9. (RE-I) and (FP-I) are the regions of coexisting three stationary solutions for injection locking. They include (RE-II) and (FP-II) which are the regions of bistability in the plane of parameters (η_0, Ω) for the value $\delta = -1$. These results were computed with the rate equation (RE-I , RE-II) and the Fabry-Perot (FP-I , FP-II) models for a YAG:Nd microchip laser with a cavity length $L = 0.4$ mm and a resonator loss of 2%.

by the stationary solutions of equations (2.3–2.5). In this case the two components with frequencies ω_{in} and ω_n are present. The stationary solution of equations (2.3–2.5) is analogous to the solution (3.18–3.20) of equations (3.15–3.17) for the rate-equation model:

$$N = 1 + \delta^2, \tag{4.10}$$

$$Y_1 = \eta_0 - \delta^2 - Y_2 \frac{1+\delta^2}{1+\delta_{in}^2}, \tag{4.11}$$

$$Y_2 = \frac{S^2 \Gamma^2 T_c^2}{1 + K_0^2 - 2K_0 \cos F_0}, \tag{4.12}$$

where:

$$K_0 = \exp[\Gamma T_c((1+\delta^2)/(1+\delta_{in}^2) - 1)], \tag{4.13}$$

$$F_0 = \left[\Omega - \delta + \delta_{in} \frac{1+\delta^2}{1+\delta_{in}^2}\right] \Gamma T_c. \tag{4.14}$$

The normalized intensities $Y_{1,2}$ *versus* the normalized detuning Ω were calculated using formulas (4.11, 4.12). For the case of the peak-mode injection (when the injected frequency ω_{in} is close to the frequency of the peak mode ω_n), the results of such calculations are plotted in Figure 10a. Here the normalized intensities $Y_{1,2}$ calculated with the rate equations model are also shown by dotted curves. Solid curves show corresponding results computed with the F-P-amplifier model. One can see that both models give practically the same results. In Figure 10b, the results are shown in the region of detunings Ω including side-mode injection. Here the rate-equation model written for the case of the peak-mode injection is not valid and formulas (4.11, 4.12) of the F-P model may be used. These results were calculated for the microchip YAG:Nd laser with a cavity length of 1 mm, $\delta = 0.4$, a cavity loss of 2%, a pump excess $\eta_0 - \delta^2 = 2$ and for a normalized amplitude of the injected field $S = 10$.

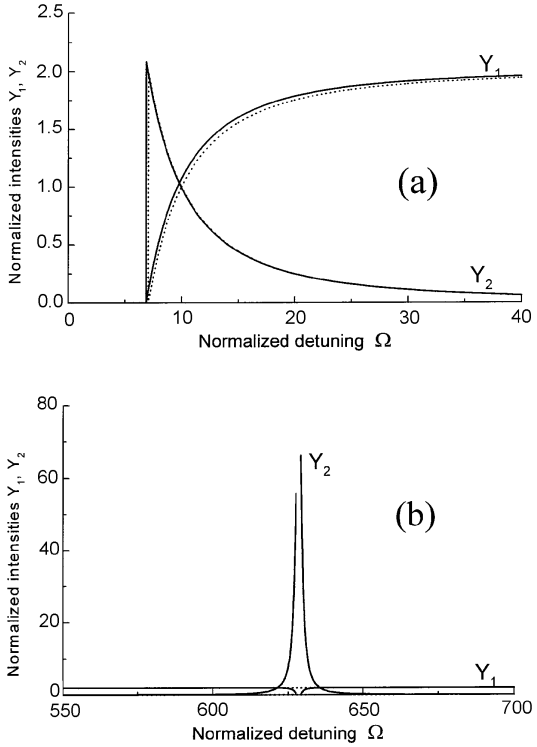

Fig. 10. Normalized intensities $Y_{1,2}$ *versus* normalized detuning Ω in the periodic beat regime for the peak-mode injection (a) and side-mode injection (b). Results for the Fabry-Perot and rate-equation models are shown, respectively, by solid and dotted curves. These results were calculated for the YAG:Nd microchip laser with a cavity length of 1 mm, $\delta = 0.4$, a cavity loss of 2%, a pump excess $\eta_0 - \delta^2 = 2$, and a normalized amplitude of the injected field $S = 10$.

5 Conclusion

We have presented a theoretical analysis of the dynamic properties of injected microchip lasers with the use of two models. The first model is based on traditional rate equations used in references model [1–11,13–28]. The second model was recently introduced f or an injected (class A) gas laser in references [35,36]. Two field components are considered which are respectively centered around the frequency of an eigenmode of the injected laser ω_n and the frequency of the injected field ω_{in}. One can write a traditional rate equation for the component at ω_n, but the equation is modified for the second component to account for Fabry-Perot filter effects. In both models, computation of locking ranges and bistability domains within the locking range has been performed and the results compared. We have also derived in both models analytic solutions for the periodic beat regime and studied its stability in the rate-equation model. It was shown that there is an asymmetric behavior of beats close to the boundaries of injection locking range. Analytic investigation of an instability region and the relaxation oscillations for the periodic beat regime has been done for the first time. In the region of instability of the periodically beat regime, numerical simulations show periodic spiking, the onset of dynamical

chaos and bistability. A comparison of results obtained for the two models leads to the conclusion that both models are equivalent for small normalized detunings Ω. However, the Fabry-Perot model describes more correctly both the peak-mode injection and side-mode injection in a broader region of detunings Ω, where it gives results which are different from those obtained with the rate-equation model. Analysis of bistability within the locking range in a microchip laser has shown that the bistability region in the F-P amplifier model is much broader. It will be interesting to experimentally test these theoretical predictions on bistability domains and temporal dynamics including chaos.

E.G. Lariontsev and I. Zolotoverkh wish to acknowledge the financial support of the Russian Foundation for Basic Research. P. Besnard and G.M. Stéphan have benefited from the financial support of the Région de Bretagne, the Conseil General of Côtes d'Armor and of the town of Lannion.

Appendix A: Equation for the field

The aim of this appendix is to describe the medium and the field from first principles in order to describe the series of approximations which are necessary to obtain our basic equations. The main problem is to find a criterion to decide if the field can be represented by a single component in the frame of the Slowly-Varying Envelope Approximation (SVEA) or by two or more components. The SVEA mixes the time and the frequency domains and brings a limitation to the precision with which the response of a physical device to an excitation can be calculated. In the following we will show that this precision depends upon the dispersion of the response function of the excited device. In our particular case, the device is the laser, the excitation is the injected field (spontaneous emission is neglected) and the response is the laser field. In the frequency domain, the cavity response function is found from Maxwell equations and boundary conditions on the mirrors (this is the laser Airy function). A Fourier transform leads to a field-dependent equation. In the following, we will use either the frequency ν or the angular frequency ω such that: $\omega = 2\pi\nu$. Transverse effects will be neglected. The field $E(t)$ in the time domain is written in complex notation. Introducing the frequency components $E(\omega)$, the Fourier relation writes:

$$E(t) = \int_0^\infty E(\omega)e^{i\omega t}d\nu = \sum_m e^{i\omega_m t}\mathcal{E}_m(t) + C.C. \quad \text{(A.1)}$$

where:

$$\mathcal{E}_m(t) = \int_{\nu_m-\delta\nu/2}^{\nu_m+\delta\nu/2} E(\omega)e^{i(\omega-\omega_m)t}d\nu. \quad \text{(A.2)}$$

The discrete sum contains the slowly envelopes $\mathcal{E}_m(t)$, each of which being centered around a frequency. The interval $\delta\nu$ is fixed by the data of the problem. In this paper we examine the case of a single mode laser field and an injected field together with other spectral components which are non-linearly generated. All these components span a frequency interval $\Delta\nu$. If the properties of the amplifying medium (gain and refraction index) and of the cavity (round trip phase) do not change appreciably inside $\Delta\nu$, one can take $\delta\nu = \Delta\nu$, *i.e.*, a single component $\mathcal{E}(t)$. Otherwise, one should keep as many components as necessary. The problem is to find a criterion following which one can use a single component or not. Let $\mathcal{E}_1(\nu)$ be the internal laser field component at frequency ν on the mirror which corresponds to the injected source $s(\nu)$. $\mathcal{E}_1(\nu)$ is obtained from Maxwell equations and boundary conditions on the cavity mirrors:

$$\mathcal{E}_1(\nu)(1 - r_1r_2e^{g-i\phi}) = s(\nu), \quad \text{(A.3)}$$

where r_1r_2 represents the round-trip losses. We will take $r_1r_2 = e^{-L}$. The gain g and the cumulated round-trip phase ϕ are both frequency dependent: $\phi = 2\pi\nu 2nd/c$. The gain g and the refraction index n are both saturated quantities. The source $s(\nu)$ corresponds to the spontaneous emission and/or to the injected field component. A Fourier transform gives the corresponding field in the time domain:

$$s(t) = \int_0^\infty \mathcal{E}_1(\nu)(1 - e^{g-L-i\phi})e^{2i\pi\nu t}d\nu. \quad \text{(A.4)}$$

We will consider one field component centered around a reference frequency ν_0, in the frame of the SVEA and such that:

$$s(t) = s_0(t)e^{2i\pi\nu_0 t}, \quad \text{(A.5)}$$

$$E(t) = \mathcal{E}_1(t)e^{2i\pi\nu_0 t}. \quad \text{(A.6)}$$

In the case where the considered frequency interval is small enough, the quantity:

$$a(\nu) := 1 - e^{g-L-i\phi}, \quad \text{(A.7)}$$

can be expanded in a Taylor series around ν_0:

$$a(\nu) = a(\nu_0) + (\nu-\nu_0)a'(\nu_0) + \frac{1}{2}(\nu-\nu_0)^2a''(\nu_0) + \cdots, \quad \text{(A.8)}$$

where $a'(\nu_0)$ and $a''(\nu_0)$ are the derivatives of $a(\nu)$ at $\nu = \nu_0$ with respect to ν. The crucial point will be the rate of convergence of this series. One obtains:

$$s_0(t) = \int_0^\infty \mathcal{E}_1(\nu)[a(\nu_0) + (\nu-\nu_0)a'(\nu_0) + \frac{1}{2}(\nu-\nu_0)^2a''(\nu_0) + \cdots]e^{i(\omega-\omega_0)t}d\nu, \quad \text{(A.9)}$$

$$s_0(t) = a(\nu_0)\mathcal{E}_1(t) - \frac{i}{2\pi}a'(\nu_0)\frac{d\mathcal{E}_1(t)}{dt} - \frac{1}{8\pi^2}a''(\nu_0)\frac{d^2\mathcal{E}_1(t)}{dt^2} + \cdots \quad \text{(A.10)}$$

When the convergence of the series is fast enough, it can be truncated and one obtains the time-varying differential equation:

$$\frac{d\mathcal{E}_1}{dt} = 2i\pi\frac{s_0}{a'(\nu_0)} - 2i\pi\frac{a(\nu_0)}{a'(\nu_0)}\mathcal{E}_1. \quad \text{(A.11)}$$

The simplest dynamic equation for the field thus writes:

$$\frac{d\mathcal{E}_1}{dt} = 2i\pi\frac{s_0 e^{(L-g+i\phi_0)}}{-g'+i\phi_0'} - 2i\pi\frac{e^{(L-g+i\phi_0)}-1}{-g'+i\phi_0'}\mathcal{E}_1. \quad \text{(A.12)}$$

One sees that such an equation has a precision limited by the complex dispersion of the medium. A stationary regime can exist only when $a(\nu)$ is frequency-independent (*i.e.* $s_0(t) = a(\nu_0)\mathcal{E}_1(t)$). The criterion for the field to be represented by a single component in the SVEA is:

$$|a'(\nu_0)| \gg \frac{1}{2}(\nu-\nu_0)|a''(\nu_0)| \gg \frac{1}{6}(\nu-\nu_0)^2|a'''(\nu_0)|\cdots, \quad \text{(A.13)}$$

and thus the above equation holds if:

$$|-g'+i\phi_0'| \gg 1/2(\nu-\nu_0)|[-g''+i\phi_0''+(-g'+i\phi_0')^2]|. \quad \text{(A.14)}$$

We will later introduce expressions for g and ϕ_0 and their derivatives in this equation. If the above criterion is not fulfilled for one component, one has to divide the frequency range into as many intervals as necessary and write an equation for each field envelope.

In the mean-field approximation, one needs an equation for the mean field $\mathcal{E}$ inside the laser. This field results from the sum of two counter propagating waves. After a round trip time, one sees that $\mathcal{E}_1(t)$ becomes $\mathcal{E}_1(t)\ e^{(g-L-i\phi)}$. Now the adiabatic approximation for the medium polarization is equivalent to the neglect of the variation of the polarizability around the frequency of interest. It follows that in this approximation, $g' = 0$ and $\phi_0' = 4\pi d/c$. Our equation for a component of the field around a given frequency will thus be:

$$\frac{d\mathcal{E}}{dt} = \frac{\kappa\mathcal{E}_{in}}{T_c} - \frac{1}{T_c}[1-e^{(-L+g-i\phi_0)}]\mathcal{E}, \quad \text{(A.15)}$$

where $\kappa\mathcal{E}_{in}$ represents the mean value of the source term during the time $T_c = 2d/c$ as expressed following the injection coefficient κ and the launched field $\mathcal{E}_{in}$.

Appendix B: Gain and dispersion of the active medium

In this appendix, we will derive expressions for the gain and for the dispersion in order to verify our preceding criterion. We will use the density matrix formalism applied to a two energy level system interacting with a field expressed with two frequency components:

$$E(t) = \mathcal{E}_1 e^{(i\omega_1 t)} + \mathcal{E}_2 e^{(i\omega_2 t)} + C.C., \quad \text{(B.1)}$$

where $\mathcal{E}_1$ and $\mathcal{E}_2$ are mutually incoherent (*i.e.* stationary) fields. The equation of evolution for the density operator $\hat{\rho}$ which locally describes the active medium writes:

$$i\hbar\frac{d\hat{\rho}}{dt} = [\hat{H},\hat{\rho}]_- + \text{phenomenological terms}, \quad \text{(B.2)}$$

where $\hat{H}$ is the Hamiltonian which will be written in the dipole approximation. Phenomenological terms describe the pumping and the different relaxation rates and result from the restriction of the atomic system to two energy levels $|u\rangle$ and $|d\rangle$ (up and down). This equation can be expended for the populations ρuu and ρ_{dd} and optical coherence terms ρ_{du}:

$$i\hbar\frac{d\rho_{dd}}{dt} = (\hat{H}\hat{\rho}-\hat{\rho}\hat{H})_{dd} + i\hbar\Lambda_d - i\hbar\gamma_d\rho_{dd}, \quad \text{(B.3)}$$

$$i\hbar\frac{d\rho_{uu}}{dt} = (\hat{H}\hat{\rho}-\hat{\rho}\hat{H})_{uu} + i\hbar\Lambda_u - i\hbar\gamma_u\rho_{uu}, \quad \text{(B.4)}$$

$$i\hbar\frac{d\rho_{du}}{dt} = (\hat{H}\hat{\rho}-\hat{\rho}\hat{H})_{du} - i\hbar\gamma_{du}\rho_{du}. \quad \text{(B.5)}$$

Terms like $i\hbar\Lambda_{(d,u)}$ describe the pumping effects. The γ's stand for the different relaxation rates. In the following, the population ρ_{dd} will be neglected because, in Nd^{3+}, γ_d is of the order of 10^9 s^{-1} and thus the lower level empties very quickly. One has: $\hat{H} = H_0 - \mu E$. H_0 is the non-perturbed Hamiltonian whose eigenvectors are $|u\rangle$ and $|d\rangle$. To these vectors correspond the energies E_u and E_d. We will take the energy difference: $E_u - E_d = \hbar\omega_0$. Equations for the matrix elements can be developed:

$$i\hbar\frac{d\rho_{uu}}{dt} = -E[\mu_{ud}\rho_{du} - \mu_{du}\rho_{ud}] + i\hbar\Lambda_u - i\hbar\gamma_u\rho_{uu}, \quad \text{(B.6)}$$

$$i\hbar\frac{d\rho_{du}}{dt} = -\hbar\omega_0\rho_{du} - E\mu_{du}\rho_{uu} - i\hbar\gamma_{du}\rho_{du}. \quad \text{(B.7)}$$

Making the SVEA for the description of the medium polarization waves one writes:

$$\rho_{du} = p_{1du}e^{i\omega_1 t} + p_{2du}e^{i\omega_2 t}. \quad \text{(B.8)}$$

Now, the population term contains low frequency components as well. We will neglect them and write $\rho_{uu} \simeq p_0$. Moreover, we will make the adiabatic approximation on the medium polarization:

$$i\hbar\frac{d\rho_{du}}{dt} = -\hbar\omega_1 p_{1du}e^{i\omega_1 t}. \quad \text{(B.9)}$$

Normalization can be achieved by using the saturation intensity: $I_s = (1/2\mu^2)(\hbar^2\gamma_{du}\gamma_u)$. We will take:

$$Y_1 = \frac{I_1}{I_s}, \quad \text{(B.10)}$$

$$Y_2 = \frac{I_2}{I_s}\,. \quad \text{(B.11)}$$

One can introduce the normalized detunings: $\delta_1 = \dfrac{\omega_1-\omega_0}{\gamma_{du}}$ and $\delta_2 = \dfrac{\omega_2-\omega_0}{\gamma_{du}}$. p_0 can be normalized by its

value at threshold. At this point, $\Lambda_{u0} = \Lambda_{uth}$ and one takes:

$$N = p_0 \frac{\gamma_u}{\Lambda_{uth}} \cdot \tag{B.12}$$

One thus obtains:

$$\frac{dN}{dt} = \frac{1}{T_1}\Big[N_0 - N(1 + \frac{Y_1}{1+\delta_1^2} + \frac{Y_2}{1+\delta_2^2})\Big], \tag{B.13}$$

with the normalized pumping rate: $N_0 = \Lambda_{u0}/\Lambda_{uth}$ and the notation $T_1 = 1/\gamma_u$. The medium polarization is expressed by the general equation:

$$P = \mathrm{Tr}[\rho\mu]. \tag{B.14}$$

Its slowly-varying envelopes $P_1(t)$ and $P_2(t)$ are defined by:

$$P = P_1(t)e^{i\omega_1 t} + P_2(t)e^{i\omega_2 t} + C.C. \tag{B.15}$$

$P_1(t)$ can be expressed as a function of N:

$$P_1(t) = -\frac{\mu^2}{\hbar}[\omega_0 - \omega_1 + i\gamma_{du}]\mathcal{E}_1 N \frac{\Lambda_{uth}}{\gamma_u} \cdot \tag{B.16}$$

It gives the polarizability α_1 (and α_2) from which the gain:

$$g_1 = \omega T_c \frac{\alpha_1^i}{2\epsilon_0} \tag{B.17}$$

and the round-trip phase:

$$\phi_1 = \omega T_c\Big[1 + \frac{\alpha^r}{2\epsilon_0}\Big] \tag{B.18}$$

can be computed (we take $T_c = 2d/c$). One finds:

$$\alpha_1 = \frac{\mu^2}{\hbar} N \frac{\omega_1 - \omega_0 + i\gamma_{du}}{(\omega_1 - \omega_0)^2 + \gamma_{du}^2} \frac{\Lambda_{uth}}{\gamma_u} \cdot \tag{B.19}$$

At threshold (at line center), $N = 1$ and g_1 compensates for losses ($g_1 = L$). One thus has the expression for the gain normalized at threshold:

$$g_1 = \frac{LN}{1+\delta_1^2} = \Gamma T_c \frac{N}{1+\delta_1^2} \cdot \tag{B.20}$$

We have introduced the notation $\Gamma = L/T_c$ which corresponds to the loss per round trip. The expression for the phase is:

$$\phi_1 = \omega_1 T_c + g_1 \delta_1. \tag{B.21}$$

The same relations hold for the second component with indices 2 instead of 1. From these relations and equation (A.15) for the field, equations (2.3, 2.4) and then (2.1) are easily recovered.

References

1. R. Lang, IEEE J. Quant. Electron. **QE-18**, 976 (1982).
2. I. Petibon, P. Gallion, G. Debarge, C. Charban, IEEE J. Quant. Electron. **QE-24**, 148 (1988).
3. K. Otsuka, S. Kobayashi, Electron. Lett. **19**, 262 (1983).
4. H. Kawagushi, K. Inoue, T. Matsuoka, K. Otsuka **QE-21**, 1314 (1985).
5. R. Hui, S. Benedetto, I. Montrosset, Opt. Lett. **18**, 287 (1993).
6. J.M. Luo, M. Osinski, Electron. Lett. **27**, 1737 (1991).
7. L. Li, IEEE J. Quant. Electron. **32**, 248 (1996).
8. Z.G. Pan, S. Jiang, M. Dagenais, R.A. Morgan, K. Kojima, M.T. Asom, R.E. Leibenguth, G.D. Guth, M.W. Focht, Appl. Phys. Lett. **63**, 2999 (1993).
9. T.B. Simpson, J.M. Liu, J. Appl. Phys. **73**, 2587 (1993).
10. J.M. Liu, T.B. Simpson, IEEE J. Quant. Electron. **30**, 957 (1994).
11. E. Cerboneshi, D. Hennequin, E. Arimondo, IEEE J. Quant. Electron. **32**, 192 (1996).
12. J. Jahanpanah, R. Loudon, Phys. Rev. A **54**, 5210 (1996).
13. T.B. Simpson, J.M. Liu, K.F. Huang, K. Tai, C.M. Clayton, A. Gavrielides, V. Kovanis, Phys. Rev. A **52**, 4348 (1995).
14. T.B. Simpson, J.M. Liu, A. Gavrielides, IEEE J. Quant. Electron. **32**, 1456 (1996).
15. T.B. Simpson, J.M. Liu, K.F. Huang, K. Tai, Quant. Semiclass. Opt. **9**, 765 (1997).
16. L. Goldberg, H.L. Taylor, J.F. Weller, D.R. Scifres, Appl. Phys. Lett. **46**, 236 (1985).
17. Y. Braiman, T.B. Kennedy, K. Wissenfeld, A. Kibnik, Phys. Rev. A **52**, 1500 (1995).
18. J. Mercier, M. McCall, Opt. Commun. **138**, 200 (1997).
19. A.P. Napartovich, D.V. Vysotsky, Opt. Commun. **141**, 91 (1997).
20. J. Sacher, D. Baums, P. Pankin, W. Elässer, E.O. Göbel, Phys. Rev. A **45**, 1893 (1992).
21. E.K. Lee, H.S. Pang, J.D. Park, H. Lee, Phys. Rev. A **47**, 736 (1993).
22. D. Boggavarapu, R.J. Grantham, Y.Z. Hu, F. Brown de Colstoun, C.W. Lowry, G. Khitrova, S.W. Koch, M. Sargent III, H.M. Gibbs, Opt. Lett. **18**, 1846 (1993).
23. V. Annovazzi-Lodi, S. Donati, M. Manna, IEEE J. Quant. Electron. **30**, 1537 (1994).
24. T.B. Simpson, J.M. Liu, A. Gavrielides, V. Kovanis, P. Alsing, Appl. Phys. Lett. **64**, 3539 (1994).
25. T.B. Simpson, J.M. Liu, A. Gavrielides, V. Kovanis, P. Alsing, Phys. Rev. A **51**, 4181 (1995).
26. T. Erneux, V. Kovanis , A. Gavrielides, P.M. Alsing, Phys. Rev. A **53**, 4372 (1996).
27. H. Li, T.L. Lucas, J.G. McInerney, IEEE J. Quant. Electron. **32**, 227 (1996).
28. B. Krauskopf, W.A. van der Graf, D. Lenstra, Quant. Semiclass. Opt. **9**, 797 (1997).
29. S. Longhi, Phys. Rev. A **56**, 2397 (1997).
30. S. Longhi, Phys. Rev. A **56**, 1553 (1997).
31. L. Gillner, G. Björk, Y. Yamamoto, Phys. Rev. A **41**, 5053 (1990).
32. A. Eschmann, C.W. Gardiner, Phys. Rev. A **54**, 3373 (1996).
33. T.C. Ralph, C.C. Harb, H.A. Bachor, Phys. Rev. A **54**, 4359 (1996).
34. C.C. Harb, T.C. Ralph, E.H. Huntington, I. Freitag, D.E. McClelland, H.A. Bachor, Phys. Rev. A **54**, 4370 (1996).
35. P. Even, K. Ait Ameur, G.M. Stéphan, Europhys. Lett. **36**, 179 (1996).
36. P. Even, K. Ait Ameur, G.M. Stéphan, Phys. Rev. A **55**, 1441 (1997).
37. G.M. Stéphan (submitted for publication).
38. M.M. Ibrahim, M.S. Ibrahim, Opt. Laser Technol. **28**, 39 (1996).